Investigating the iso-radial thermal structure of gas within Clusters of Galaxies: a multi-scale approach

H. Bourdin[1], P. Mazzotta[1], E. Rasia[2] and K. Dolag[3]

ABSTRACT

Clusters of galaxies are permeated by a hot X-ray emitting gas which thermodynamical evolution is affected by a complex baryonic physics. Related to the underlying density structure of the Intra-Cluster Medium (ICM), with spherical symmetry, gas brightness and temperature profiles within cluster samples have been extensively studied in X-ray astronomy, their shape enabling us in particular to put observational constraints on the theoretical models of cluster evolution. Profile catalogues show however a scatter which origin is likely to be related to both statistical fluctuations and intrinsic gas brightness and thermal structure within individual clusters. In order to couple 2d and radial analyses of this thermal structure, we introduce an iso-radial analysis approach of X-ray spectral-imaging, where thermal features of the ICM are enhanced by means of elliptical wavelet coefficients. We present an application of this approach to mock XMM-Newton observations of a simulated galaxy cluster sample, assuming different physics of the ICM. We show that such a scheme should enable us to investigate the relative influence of various physical processes affecting ICM thermodynamics, in particular the radiative cooling, heat conduction and star formation within cluster galaxies.

1. Introduction

Clusters of galaxies, the largest gravitationally bound structures in the Universe, are permeated by a hot X-ray emitting gas dominating their baryonic mass budget. X-ray observations performed using spatially resolved spectroscopy down to the arcsec angular resolution have recently revealed us the complex thermal structure of this Intra-Cluster Medium (ICM) (see e.g. Govoni et al. 2004; Bourdin & Mazzotta 2008; Andersson et al. 2009; Owers et al. 2009; Million & Allen 2009). As suggested by theoretical models and hydrodynamical N-body simulations, this thermal structure testifies to the thermodynamical history of the ICM submitted to competitive heating and cooling processes during its evolution, such as shock heating and mixing processes due to substructure accretion, energy feedback from active galaxies and supernovae, radiative cooling and possible thermalisation by electronic conduction.

A better knowledge of the interplay between these various physical processes might be provided by quantitative comparisons between estimates of the ICM thermal structure, in both simulated and real cluster

[1]Dipartimento di Fisica, Università degli Studi di Roma "Tor Vergata", via della Ricerca Scientifica, 1, I-00133 Roma, Italy

[2]Department of Physics, University of Michigan, Ann Arbor, MI, USA

[3]Max-Planck Institut für Astrophysik, Garching, Germany

samples. As these processes strongly depend on the intra-cluster gas density, with spherical symmetry, radial analyses of the projected brightness and temperature structure of the ICM have been widely used in X-ray astronomy (see e.g. Cavaliere & Fusco-Femiano 1976; Neumann & Arnaud 1999; Markevitch et al. 1998; De Grandi & Molendi 2002; Arnaud 2009, and references therein). Related to the shape of cluster gravitational potentials, these radial analyses enable us indeed in particular to model the 3d structure of ICM thermodynamical properties, such as gas pressure and entropy (see e.g. Voit 2005; Pratt et al. 2010; Arnaud et al. 2010). Both observations (see e.g. Solovyeva et al. 2008; Bourdin & Mazzotta 2008) and predictions from hydrodynamical N-body simulations (Dolag et al. 04) have shown however, that radial analyses of the ICM thermal structure are marginally sensitive to the strong fluctuations observed on its projected 2d structure. In order to couple radial and 2d analyses of the ICM thermal structure, we propose to measure and quantify this structure through an iso-radial analysis scheme, where thermal features are enhanced by means of elliptical wavelet coefficients.

We present an application of this analysis scheme to mock XMM-Newton observations of a simulated galaxy cluster sample, assuming three different physics of the ICM. The simulated data set is presented in Sect. 2, the analysis technique is detailed in Sect. 3, the results obtained are presented in Sect. 4 and followed by our conclusions.

2. The data set: mock X-ray observations of galaxy clusters

2.1. Simulating the intra-cluster gas thermodynamics within clusters of galaxies

We extracted a sample of five massive and hot galaxy clusters (kT=8.96, 7.68, 9.39, 7.05, 7.43 keV) from hydrodynamical N-body simulations running in cosmological context, assuming three different physics of the Intra-Cluster Medium (ICM): i) a purely adiabatic medium, ii) a radiating (cooling) ICM undergoing heating from star formation, iii) a radiating ICM undergoing star formation and thermalising assuming strong electronic conduction. More details about these cluster simulations are provided in Dolag et al. (2004).

After having placed our cluster sample to a nearby redshift range of z=[.06,.08], we projected its X-ray brightness and temperature along the line of sight, as shown in Fig. 1. Showing a spherical morphology, these clusters are continuously accreting substructures from the cosmic web. The five clusters simulated with cooling and star formation processes show a more regular brightness and thermal structure than clusters simulated assuming a purely adiabatic ICM, as a result of gas heating in the cool infalling sub-clusters. The ICM thermal structure is even more regular when adding electronic conduction. The residual cool peaks observed on the maps are simulation artifacts.

2.2. Emulating X-ray observations

Combining bremsstrahlung emission from the hot intra-cluster plasma and heavy element emission lines, X-ray emission from galaxy clusters is characterised by low statistics, leading to a photon detection

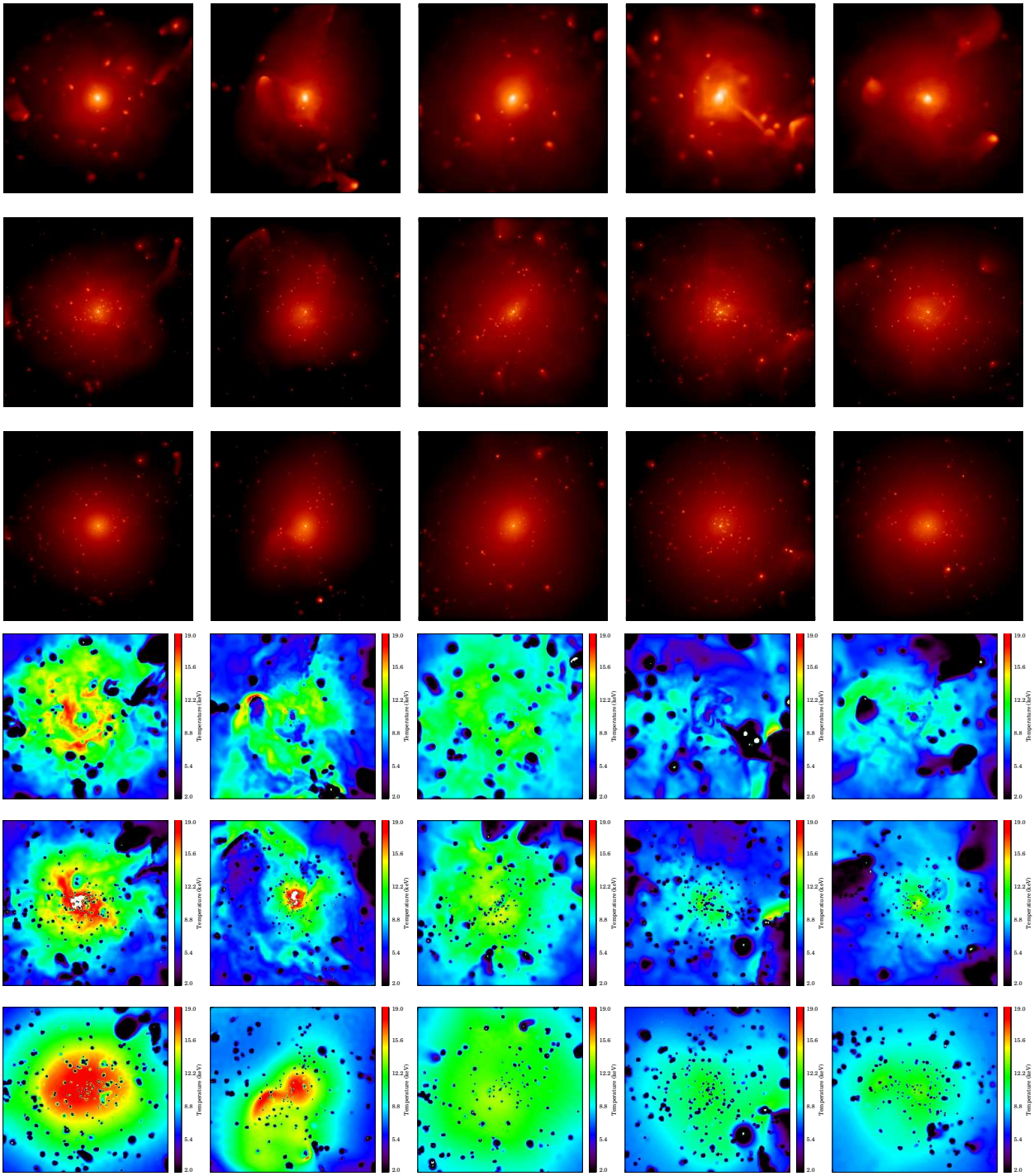

Fig. 1.— Projected X-ray brightness (top panel) and temperature (bottom panel) of the ICM in our simulated galaxy cluster sample. Five galaxy clusters (from left to right) are simulated assuming three different ICM physics. From top to bottom: i) purely adiabatic medium, ii) radiating ICM undergoing star formation heating, iii) radiating ICM undergoing star formation and thermalising through strong electronic conduction .

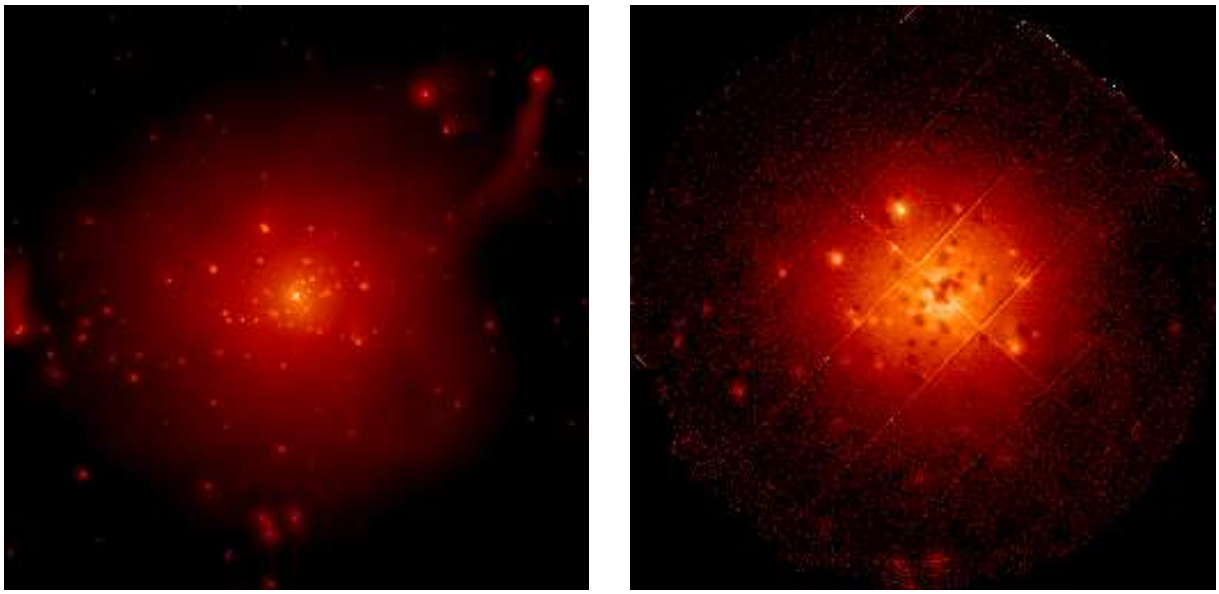

Fig. 2.— Mock X-ray observation of the first galaxy cluster in our sample, simulated assuming radiating ICM with star formation. Left: Projected ICM emissivity (same as left cluster in Fig. 1). Right: Simulated XMM-Newton photon image at the European Photon Imaging Camera. We notice that the faint outermost substructures are no longer observable through the instrument, since dominated by background noise including both instrumental and astronomical components.

with shot noise. To mimic spectral-imaging observations of our simulated galaxy clusters, we generated a set of 25 ks XMM-Newton observations at the European Photon Imaging Camera (EPIC, see also Fig. 2). To do so, we first draw a random set of photons emitted in each energy band and spatial resolution element, then emulate the various distortions experienced by X-ray photons during their travel from emission in the intra-cluster gas, to detection on spectral-imaging CCDs equipping the telescope focal planes. This includes in particular a redshift distortion of the emission spectrum, foreground emission components and photon absorption from the Galaxy, photon absorption by the spatially variable effective area of the telescopes, instrumental response and false detection due to detector interactions with high energy particles. More details about these mock X-ray observations can be found in Rasia et al. (2008).

3. Data analysis: X-ray spectral-imaging in elliptical coordinates

While X-ray telescopes can now reach a theoretical angular resolution of about one arcsec, the galaxy cluster emission is still limited by statistics. For this reason, mapping a spectroscopic observable usually requires a spatial rebinning, introducing a competition between the angular resolution to which the searched observable –presently the ICM temperature– is mapped, and the precision of its local estimates. Various denoising approaches have been proposed so far to solve this compromise, including spatially adaptive fil-

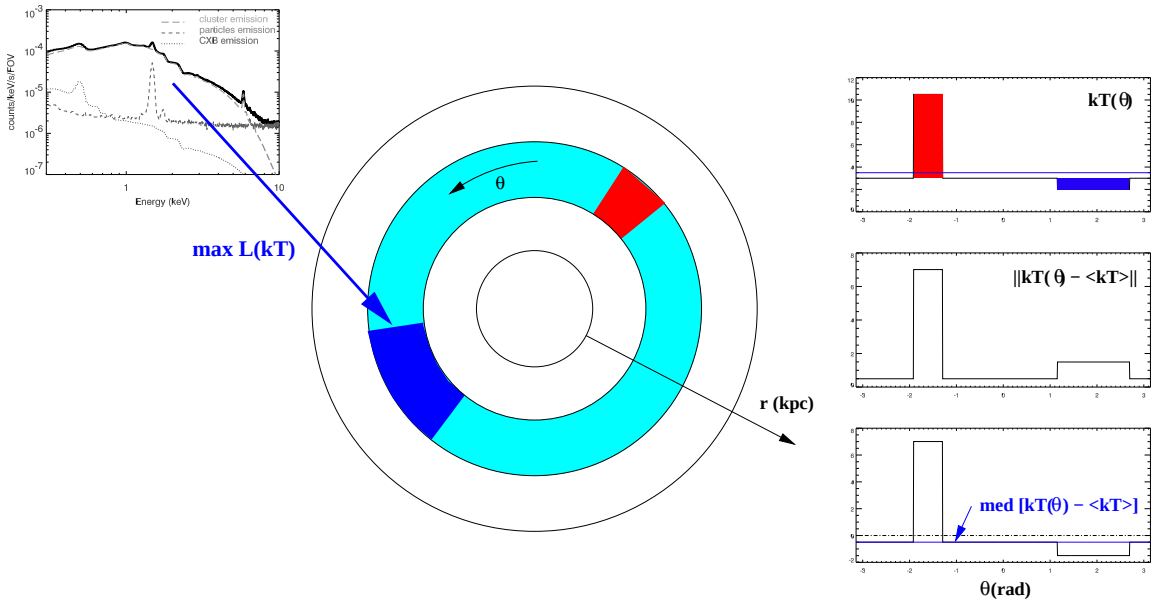

Fig. 3.— Spectral-imaging in elliptical coordinates. The projected thermal structure of the ICM is searched within various sections of a given cluster annulus, by means of likelihood maximisations of an emission spectrum. In the coloured annulus, the red spot corresponds to a hotter region than average annulus temperature, the blue spot to a colder region. Right plots, from top to bottom: i) iso-radial thermal signal kT(θ) associated with the coloured annulus; ii) iso-radial energy of the thermal signal, as defined in Eq. (2); iii) average (dot-dashed line) and median thermal signal (blue line), as defined in equation (3).

tering or wavelet thresholding (see e.g. Bourdin & Mazzotta 2008, and references therein). We here propose to adapt a multi-scale approach of spectral-imaging to the iso-radial analysis of ICM thermal structure.

3.1. Local spectroscopic estimate of the ICM temperature

As shown on Fig. 3, we investigate the projected thermal structure of ICM in a set of concentric annuli with fixed width δr, corresponding to a physical intra-cluster distance $r_o \pm \delta r$. For each annulus, we estimate various spectroscopic temperatures $\mathrm{kT}(\theta, a, r_o) \pm \sigma_{\mathrm{kT}}(\theta, a, r_o)$, by means of likelihood maximisations of an ICM emission spectrum $f(\mathrm{kT}, e)$, within annular sections of lengths $s = 2^a$, $a = \{1, ..n\}$. Implemented from the Astrophysical Plasma Emission Code (APEC, Smith et al. 2001), this emission model takes into account the temperature dependence of bremsstrahlung continuum and emission lines of ICM emissivity. It is corrected for source redshift, Galactic neutral hydrogen absorption, X-ray foreground and background extended emissions as well as instrumental background noise, mirror effective area and detector energy response. This likelihood maximisation of is performed following the same procedure as detailed in Bourdin et al. (2004), leading to a close to Minimum Variance Bound estimate in standard observing conditions.

3.2. Iso-radial wavelet analysis of the thermal structure

Re-convolving n times the thermal signal $\mathrm{kT}(\theta, a, r_o)$ obtained at each scale a, with a top-hat kernel of width 2^a, we are left with a 1d filtering of the iso-radial ICM thermal structure, by means of B-spline analysis functions of order n (Curry & Schoenberg 1966). This multi-scale analysis can be projected in the scale-space by means of B-spline wavelet coefficients directly obtained by differences between annuli convolved at successive scales, following approach of the Isotropic Undecimated Wavelet Transform (Starck et al. 2007). Following this scheme, the thermal structure is separated from average temperature in each annulus, $< \mathrm{kT}(r_o) >$, and coded as wavelet coefficients $\mathrm{W_{kT}}(\theta, a, r_o)$ with characteristic intra-cluster sizes $s = 2^a$:

$$\mathrm{kT}(\theta, r_o) =< \mathrm{kT}(r_o) > + \sum_a \mathrm{W_{kT}}(\theta, a, r_o), \tag{1}$$

This projection enables us to denoise the thermal signal from k-σ thresholding of the wavelet coefficients. To do so, we must estimate the variance of our B-spline wavelet coefficients at each scale a, which is done by applying a numerical correcting factor to the variance of the local temperature estimates $\sigma^2_{\mathrm{kT}}(\theta, a, r_o)$. Assuming a white gaussian noise, this factor is obtained from ratios of impulse responses of the wavelet filter at scale a to the top-hat smoothing filter associated the angular partitioning of each annulus.

In the following, we will quantify the energy of thermal structure detected in each annulus from the L2-norm of the denoised wavelet coefficients:

$$\| \mathrm{kT}(\theta, r_o) - < \mathrm{kT}(r_o) > \| = \sqrt{\sum_a \mathrm{W_{kT}}(\theta, a, r_o)^2}, \tag{2}$$

We will further estimate the signed contribution of the thermal structure to the average temperature measured in each annulus, $< \mathrm{kT}(r_o) >$, from the median of wavelet coefficients:

$$med\,[\mathrm{kT}(\theta, r_o) - < \mathrm{kT}(r_o) >] = med\left[\sum_a \mathrm{W_{kT}}(\theta, a, r_o)\right]. \tag{3}$$

4. Results

We analyse mock X-ray observations of the galaxy cluster sample presented in section 2 and present our results in Fig. 4. These plots show the temperature profile and multi-scale analysis of the iso-radial thermal structure of ICM in our sample. In Fig. 5, we further report similar results obtained from a secondary analysis of the sample, performed after suppressing the most prominent sub-structures of brightness maps.

We plot for each cluster sample –i) adiabatic medium, ii) ICM with cooling and star formation (hereafter CSF), iii) ICM with cooling, star formation and conduction (hereafter CSFC)–, the temperature profile

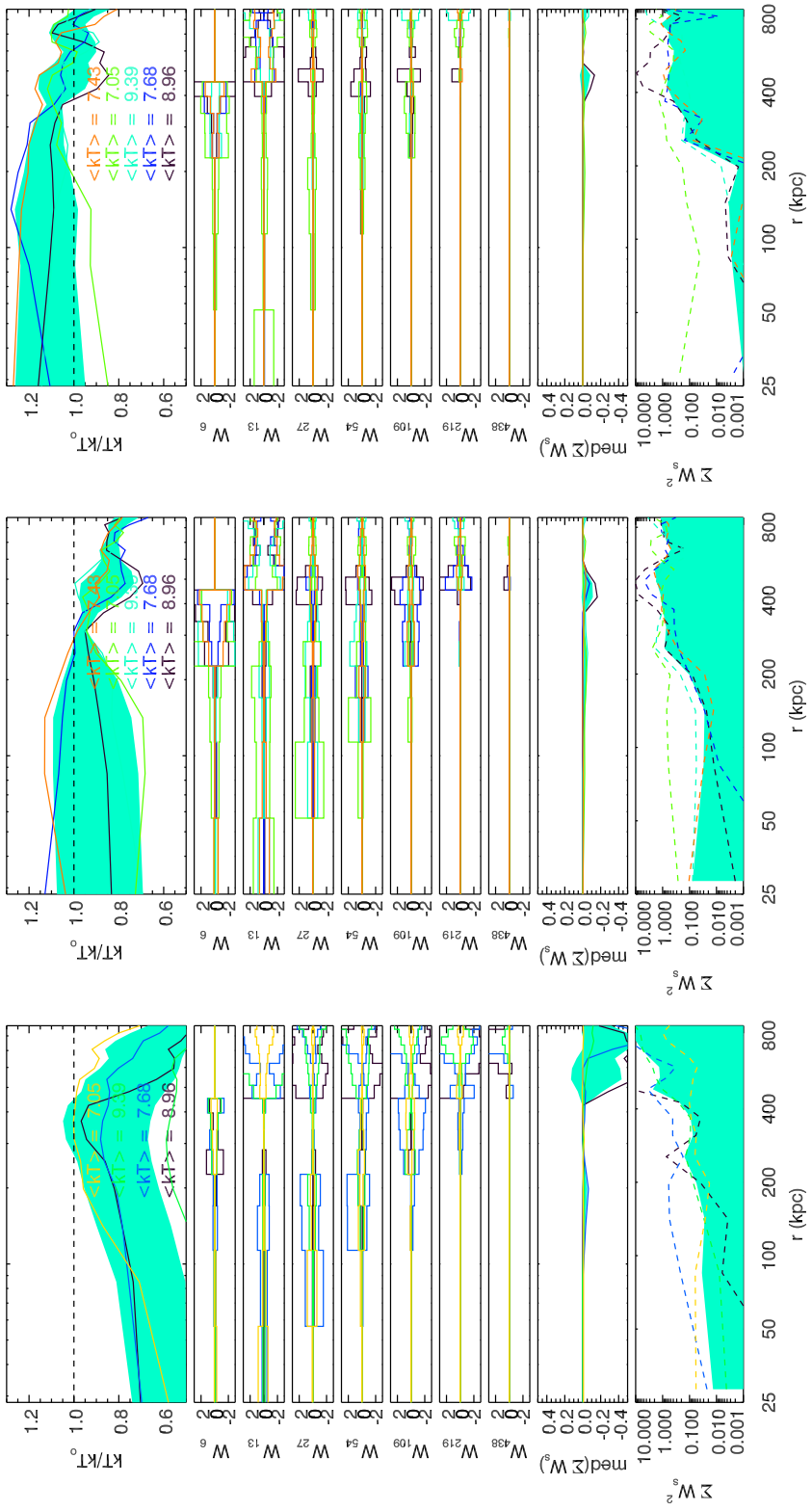

Fig. 4.— Iso-radial thermal structure of the ICM in our simulated galaxy cluster sample. From left to right: i) purely adiabatic medium, ii) radiating ICM undergoing star formation (CSF), iii) radiating ICM undergoing star formation and strong electronic conduction (CSFC). From top to bottom on the plots: temperature profile of each cluster (colour code), and dispersion of temperature profiles in the sample (blue shaded area). Angular sums of wavelet coefficients associated with thermal structure, computed on seven scales corresponding to a distance range of 6-438 kpc (see also coefficient indexes for intermediate distances in the wavelet transform). Median of the coefficients and total energy of the iso-radial wavelet transforms.

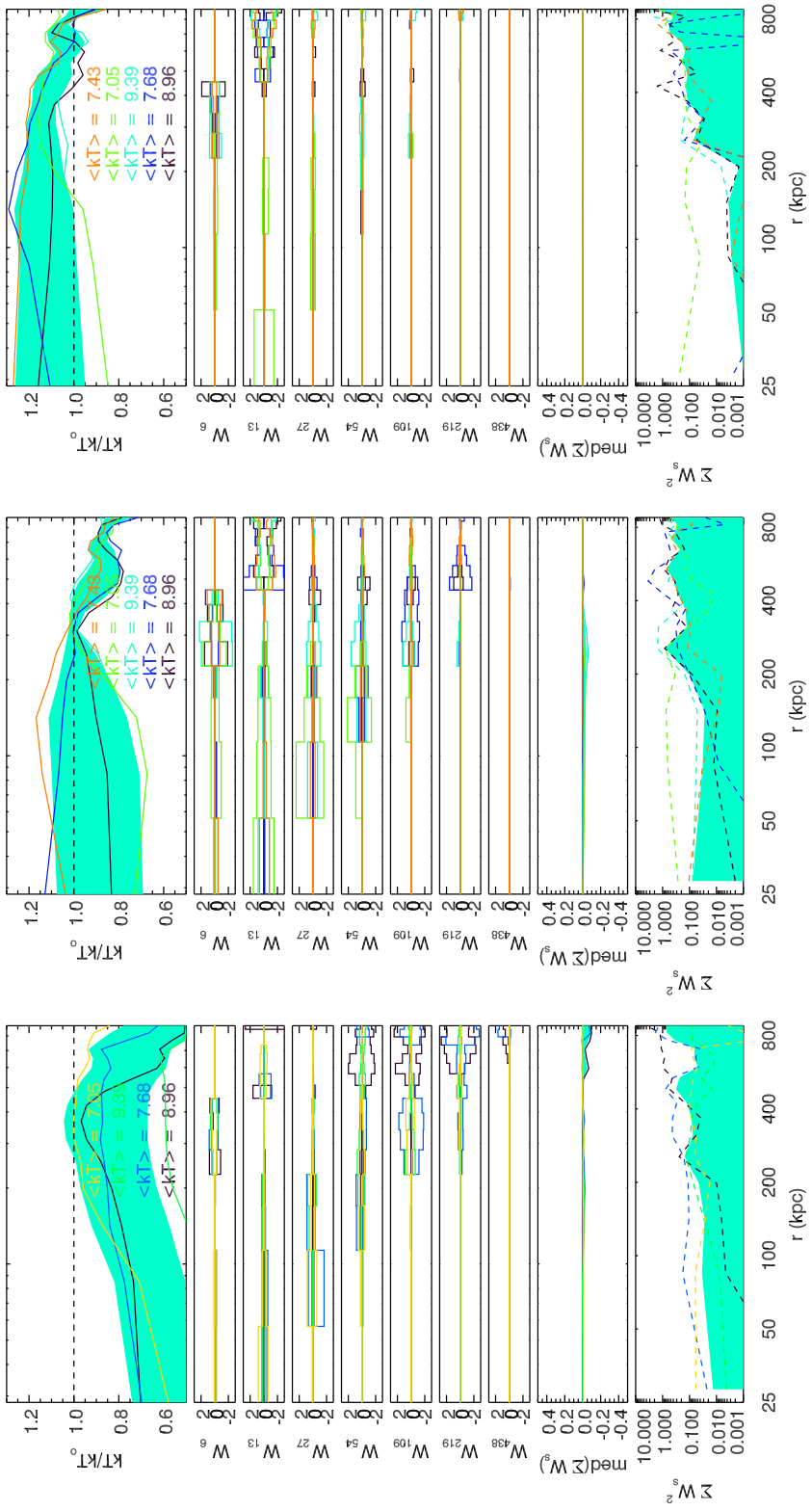

Fig. 5.— Same as Fig. 4 as for residual ICM emissivity obtained after suppression of the infalling sub-clusters on brightness maps.

of each cluster, and the dispersion of temperature profiles in the sample. The angular sums of wavelet coefficients associated with thermal structure, $S(r) = \sum_\theta W_{kT}(\theta, a, r)$, has been computed within 16 cluster annuli covering the radius range r=[28,900] kpc, and reported below the profiles. The total energy and median of these coefficients, as defined in Eq. (2) and (3) are further reported below the wavelet transforms.

We firstly observe that the wavelet transform associated with the CSFC cluster sample show lower amplitude coefficients than wavelet transforms associated with the adiabatic and CSF cluster samples, in particular at large scales ($s > 30$kpc). As observed on the temperature maps of first panel, the thermal conduction has indeed erased the ICM thermal structure in the CFSC sample. Wavelet transforms associated with the adiabatic and CSFC clusters also show significant differences between one another, the largest amplitude coefficients being located at smaller radii in the CSFC case than in the adiabatic case. Consistent with a visual inspection of temperature maps of Fig. 1, this behaviour reflects the predominance of galaxy feedback effects on the ICM thermal structure in the innermost regions of the CSFC clusters, while sub-cluster accretion has strongly disturbed the outskirts of adiabatic clusters. As infalling sub-clusters are cooler than their accreting clusters, the median of the overall wavelet transform further show us that their thermal contribution has lowered the overall temperature measured at largest radii in the temperature profiles. This contribution can be suppressed by masking sub-structures on the brightness maps, as shown on plots of Fig. 5. Discrepancies observed between the three wavelet transform can finally be quantified by measuring their total energy, this quantity showing a radial increase in the case of adiabatic clusters, a more regular radial dependence in the case of CSF clusters, and lowest values in the innermost part of the CSFC clusters.

5. Conclusion

We proposed to a multi-scale approach enabling us quantify the iso-radial thermal structure of hot gas within galaxy clusters. Following framework of the Isotropic Undecimated Wavelet Transform, this approach provides us a complementarity between this thermal structure and the average radial values measured on the temperature profiles. Our multi-scale analysis being performed from a radial partition of the sky plane in physical intra-cluster distances, the thermal features observed in different targets may be associated to characteristic distances, typically measured in kpc, and compared with each other.

From our analysis of mock X-ray observations of a nearby sample of galaxy clusters, we show that applying this approach to real cluster samples should enable us to investigate the contribution of accreted material in the dispersion observable on temperature profiles, in particular to the cluster outskirts. We further show that physical processes at play within the ICM, in particular the efficiency of electronic conduction, should be constrained from reasonable time X-ray observations of hot and massive galaxy clusters. Assuming ICM thermal fluctuations to be generated following an ergodic process, performing such measurements within individual clusters may provide us insights about the origin of dispersions observed between temperature profile of cluster catalogues (see e.g. Vikhlinin et al. 2005; Pratt et al. 2007), in particular in the innermost cluster regions experiencing strong gas colling and galaxy feedback, and outermost regions undergoing sub-cluster accretion.

REFERENCES

Andersson, K., Peterson, J. R., Madejski, G., & Goobar, A. 2009, ApJ, 696, 1029

Arnaud, M. 2009, A&A, 500, 103

Arnaud, M., Pratt, G. W., Piffaretti, R., Böhringer, H., Croston, J. H., & Pointecouteau, E. 2010, A&A, 517, A92+

Bourdin, H., & Mazzotta, P. 2008, A&A, 479, 307

Bourdin, H., Sauvageot, J., Slezak, E., Bijaoui, A., & Teyssier, R. 2004, A&A, 414, 429

Cavaliere, A., & Fusco-Femiano, R. 1976, A&A, 49, 137

Curry, H. B., & Schoenberg, I. J. 1966, Journal d'Analyse Mathématique, 17, 71

De Grandi, S., & Molendi, S. 2002, ApJ, 567, 163

Dolag, K., Jubelgas, M., Springel, V., Borgani, S., & Rasia, E. 2004, ApJ, 606, L97

Govoni, F., Markevitch, M., Vikhlinin, A., van Speybroeck, L., Feretti, L., & Giovannini, G. 2004, ApJ, 605, 695

Markevitch, M., Forman, W. R., Sarazin, C. L., & Vikhlinin, A. 1998, ApJ, 503, 77

Million, E. T., & Allen, S. W. 2009, MNRAS, 399, 1307

Neumann, D. M., & Arnaud, M. 1999, A&A, 348, 711

Owers, M. S., Nulsen, P. E. J., Couch, W. J., & Markevitch, M. 2009, ApJ, 704, 1349

Pratt, G. W., Arnaud, M., Piffaretti, R., Böhringer, H., Ponman, T. J., Croston, J. H., Voit, G. M., Borgani, S., & Bower, R. G. 2010, A&A, 511, A85+

Pratt, G. W., Böhringer, H., Croston, J. H., Arnaud, M., Borgani, S., Finoguenov, A., & Temple, R. F. 2007, A&A, 461, 71

Rasia, E., Mazzotta, P., Bourdin, H., Borgani, S., Tornatore, L., Ettori, S., Dolag, K., & Moscardini, L. 2008, ApJ, 674, 728

Smith, R. K., Brickhouse, N. S., Liedahl, D. A., & Raymond, J. C. 2001, ApJ, 556, L91

Solovyeva, L., Anokhin, S., Feretti, L., Sauvageot, J. L., Teyssier, R., Giovannini, G., Govoni, F., & Neumann, D. 2008, A&A, 484, 621

Starck, J.-L., Fadili, J., & Murtagh, F. 2007, IEEE Transactions on Image Processing, 16, 2007

Vikhlinin, A., Markevitch, M., Murray, S. S., Jones, C., Forman, W., & Van Speybroeck, L. 2005, ApJ, 628, 655

Voit, G. M. 2005, Reviews of Modern Physics, 77, 207